TOWARDS AERODYNAMIC CONTROL OF MINIATURE ROCKETS WITH MEMS CONTROL SURFACES

Ahad M. Rauf, Brian G. Kilberg, Craig B. Schindler, Sang A Park, and Kristofer S. J. Pister
Berkeley Sensor & Actuator Center
University of California, Berkeley, California, USA

ABSTRACT

We demonstrate a MEMS-actuated aerodynamic control surface integrated into an untethered 16.9 g, 20 cm rocket. The system's flight performance was characterized inside a wind tunnel. The actuator system generates 3.6 µNm of torque about the rocket's body axis in 13.3 m/s airflow with 5.1° angle of attack, inducing a maximum roll velocity of 100°/s. This is the first electrostatic inchworm motor-actuated MEMS control surface to perform aerodynamic maneuvers in a self-contained rocket body.

KEYWORDS

MEMS Airfoils, Miniature Rockets, Micro-Air Vehicles, Electrostatic Inchworm Motors

INTRODUCTION

Miniature autonomous rockets provide a natural solution to problems such as micro-air vehicle (MAV) swarm interception and rapid area surveillance, where conventional systems with larger sizes or ballistic trajectories tend to be either expensive or unportable [1], [2]. These rockets benefit from recent improvements in battery energy density and the decreasing size, power, and cost of digital computation and sensors, which could enable low-cost, highly maneuverable autonomous MAVs with size scales <15 cm.

The smallest guided rocket currently in production is the US Navy's 64 cm long, 57 mm diameter Spike missile. Miniaturizing rocket guidance systems even further will require reducing the size of rocket propellant systems, control and communication electronics, and control surface mechanisms. Previous research has already miniaturized composite propellant rocket motors [3]–[4] and developed 2x3 mm^2 wireless system-on-chips that can be used as miniaturized avionics and telemetry platforms [5]. These technologies are developed enough that they could be feasibly integrated into a microrocket in their current state.

Recent research efforts have also focused on developing miniaturized control surfaces using microelectromechanical systems (MEMS) technologies such as microbubble actuator arrays, piezoelectric actuators, and electrostatic inchworm motors [6]–[9]. Kilberg et al. have previously demonstrated MEMS control surfaces based on electrostatic inchworm motors, which could be viable for controlling cigarette-sized microrockets due to their small sizes and efficient operation [8], [9]. This mechanism enables 100x smaller device scales compared to previous MEMS aerodynamic actuators [6] as well as 5x lower drive voltages and 2x larger actuator displacements compared to previous piezoelectric aerodynamic actuators [7].

This work presents further improvements towards miniaturizing this MEMS-actuated control surface design.

Figure 1: The fully assembled rocket, consisting of a MEMS control surface and its 2x4 mm^2 steel airfoil, a single-cell LiPo battery, and control electronics.

It highlights changes made in the assembly process to prevent out-of-plane forces from dislocating silicon mechanisms, as well as a higher-density electrostatic inchworm motor design. This paper also discusses the procedure for integrating the MEMS actuator into a fully contained 16.9 g, 20 cm rocket system, which is composed of a battery, wireless sensor node, IMU, and high voltage buffer board for running the inchworm motors at 80 V.

THEORY AND DESIGN

Aerodynamics and Airfoil Design

Most aircraft use control surfaces such as ailerons, elevons, and canards to control their trajectories. For small angles of attack ($\alpha < 15°$), the lift force F_l produced by these airfoils can be modeled using thin airfoil theory.

$$F_l = \frac{1}{2}\rho v^2 2\pi\alpha A \tag{1}$$

where ρ is the density of air, v is the airflow velocity, and A is the airfoil's area. Our control surface uses electrostatic inchworm motors and rotary pin joints to rotate a 2x4x0.03 mm^3 steel foil airfoil. Previous simulations showed that control surfaces generating ~10 mN of lift force suffice to control a millimeter-scale rocket [2]. With our airfoil's dimensions, we can achieve this lift force at an airflow velocity of v = 35 m/s, and we've previously observed in simulation that our rocket can readily achieve this speed throughout most of its flight path [8].

The resulting aerodynamic lift force applies a torque on the rocket, providing us with a method of controlling roll and yaw.

$$\tau_{roll} = F_l(r + r_{CoP}) \tag{2}$$
$$\tau_{yaw} = F_l d_{CoP} \tag{3}$$

where r is the rocket's body radius (7.5 mm), r_{CoP} is the radial distance from the base of the fin to the fin's center of pressure, and d_{CoP} is the distance between the rocket's center of gravity and the fin's center of pressure (defined by the fin's quarter-chord within thin airfoil theory). Equations 2 and 3 allow us to control roll and yaw with one aerodynamic airfoil, and adding multiple airfoils around the rocket's circumference gives us full control over roll, pitch, and yaw.

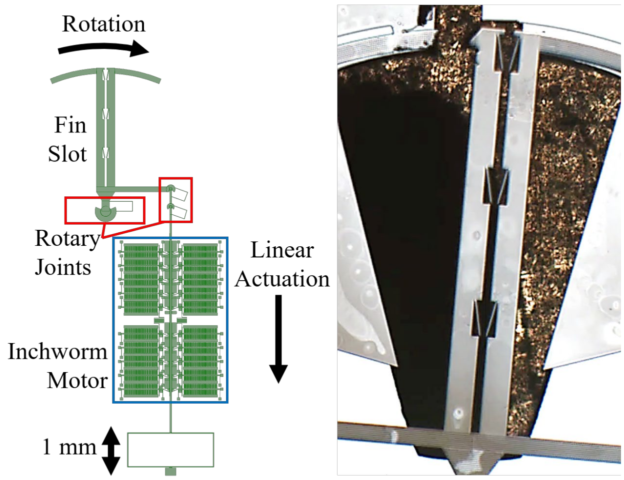

Figure 2: (Left) Schematic of half of the MEMS actuator mechanism. The inchworm motor linearly actuates the rotary pin joints, which rotate the airfoil slot. (Right) A microscopic photograph of the airfoil slot after rotation.

MEMS Actuator Mechanism

The MEMS actuator, fabricated in a simple 2-mask silicon-on-insulator (SOI) process, comprises a pair of electrostatic inchworm motors and rotary pin joints. The inchworm motors pull on a lever arm attached to the airfoil slot, which rotates the airfoil (Figure 2). We applied the higher-density electrostatic inchworm motor design described in [10] to increase our force density by 65% compared to previous work done in [9], as measured by the ratio between the capacitive finger overlap area and the entire motor's layout area. This redesign allowed us to shrink the MEMS device's area by 21% from 9x7 mm^2 to 5x9 mm^2, realizing our design goal of a MEMS actuator that can fit on a 6 mm diameter rocket [8].

Previous work has attempted to prevent out-of-plane forces from dislocating the silicon mechanisms by gluing a small silicon piece over the rotary pin joints [9]. One problem we found with this process was that commercial silver epoxy or superglue would often wick a significant distance from its initial application position, immobilizing silicon mechanisms. To solve this issue, we added extra slots to either side of the MEMS device, where we slotted in a bracket that lay over the lever arm and pin joint structures (Figure 3). The bracket is secured via epoxy only at the sides to prevent wicking from affecting any mobile MEMS components. We fabricated the brackets using the same 2-mask SOI process, and we observed no degradation in device performance after placing the bracket.

INTEGRATED ROCKET DESIGN

MEMS Actuator Mechanism

To mount the assembled control surfaces onto the rocket, we developed a custom flexible printed circuit board with room for 4 control surfaces (Figure 3). The MEMS device substrate is electrically connected via silver epoxy to a large ground plane, and the other control signals are routed from the PCB to the control surface via standard wire bonding techniques. The assembled flexible PCB is then wrapped around a custom 3D-printed fuselage and friction fit into the rocket body (Figure 1).

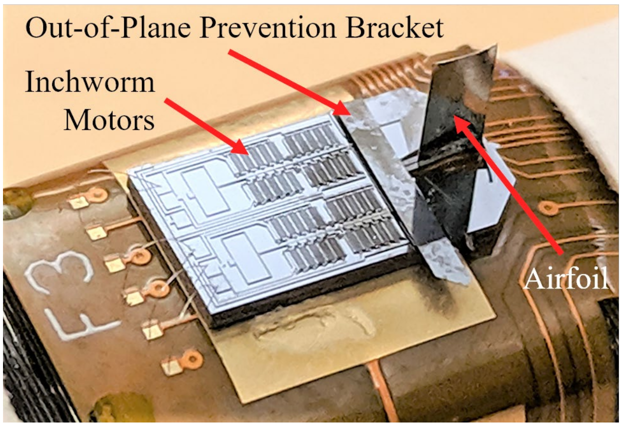

Figure 3: The assembled MEMS control surface.

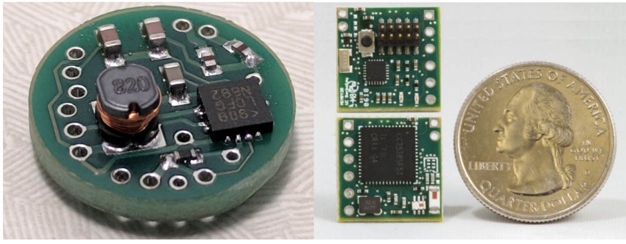

Figure 4: (Left) The 13 mm diameter high voltage buffer board. (Right) The MIMSY control and wireless node.

One problem we found in practice with this process was that any curvature in the flexible PCB or flexibility in the substrate substantially decreased our wire bonding yield. To solve this, we attached a 0.5 mm thick carbon fiber stiffener behind the ground plane before the epoxy step, which greatly improved our wire bonding yield.

Our placement of the airfoil closer to the rocket's front end follows from the design of canard guided missiles, which feature motorized frontal control surfaces and passively stabilizing tail fins. By shifting the rocket's center of pressure forward, this design model improves the rocket's response time and control surface output gain, reducing the required control surface hinge moment compared to equivalent tail fin controllers and decreasing the rocket's miss distance against mobile targets [11]. The design also facilitates rocket assembly by keeping the control surfaces and electronics far from the rocket engine.

Electronics and Controls

The inchworm motors require 45 V–110 V to operate, which poses a power supply challenge at small scales. To solve this, we developed an 80 V high voltage buffer board based on Linear Technology's LT3482 DC/DC boost converter. The board's 13 mm diameter footprint enables it to be mounted normal to the rocket's body axis, presenting a 4x area decrease and a 5 cm rocket length reduction compared to previous iterations [9] (Figure 4).

The rocket's onboard control and wireless communication are handled by the Micro Inertial Measurement System (MIMSY), a 16x16 mm^2 node with an Arm Cortex-M3 microprocessor, 802.15.4 wireless transceiver, and a 9-axis IMU [12]. Input power was supplied via a 40 mAh single-cell lithium polymer battery, which can power the IMU and a constantly running TX radio broadcast for roughly an hour after the rocket lands.

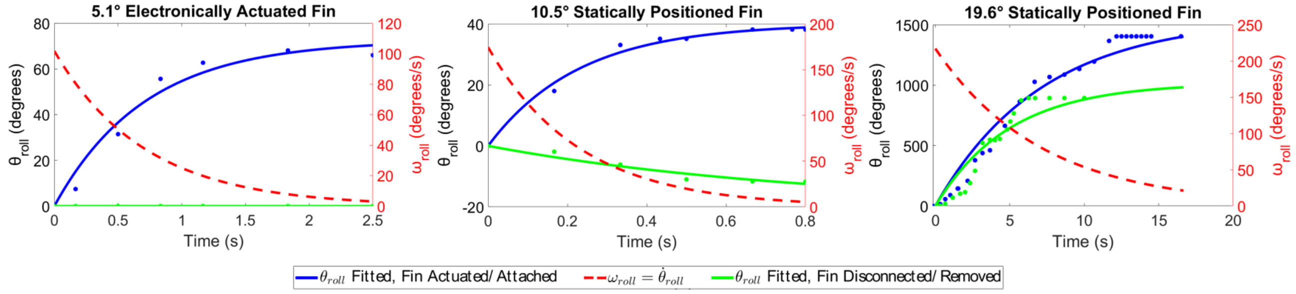

Figure 1: Roll angle vs. time data for individual rocket experiments in the wind tunnel, measured visually. The plots show the difference between the rocket's roll with and without an actuated fin. From left to right, the experiments were conducted at $K_{torsion}$ = 2.6 μNm, 4.9 μNm, and 0.51 μNm. The 5.1° and 10.5° experiments were conducted in 13.3 m/s airflow while the 19.6° experiment was conducted in 20.1 m/s airflow, which explains the latter's large roll angles.

AERODYNAMIC PERFORMANCE

The system was tested inside a wind tunnel with 13.3 m/s airflow. Because the rocket's moment of inertia about its roll axis is much smaller than about its pitch or yaw axes, for ease of measurement we focused on measuring the roll generated from the airfoil's aerodynamic lift. The full testing setup is shown in Figure 6. The rocket's vertical suspension by tensioned string in the wind tunnel allowed us to model the system as a torsional pendulum.

$$\sum\tau = I\ddot{\theta} = \tau_{roll} - K_{torsion}\theta \quad (4)$$

$$K_{torsion} = \frac{GJ}{L} \quad (5)$$

where I the moment of inertia along the roll axis, $K_{torsion}$ is the suspension string's torsional coefficient, G is the string's shear modulus, J is the string's second moment of area ($J = \pi r^4/2$ for a circular cross-section), and L is the string's length. We used 0.005" diameter Berkley XLPS2-15 fishing line for our suspension string. To characterize the fishing line's shear modulus, we measured its period of oscillation as a torsional pendulum given a test load of known moment of inertia. We fitted this data to Equation 5 to show that $G = 6.9\,GPa$ for our fishing line with an r^2 value of 0.96, indicating high convergence to the theory.

To measure the control surface's output torque τ_{roll}, we measured the rocket's equilibrium position about its roll axis at different wind speeds and angles of attack (Figure 5). We tested fins at three different angles of attack: the 5.1° fin is electronically actuated, while the 10.5° and 19.6° fins are glued into place as control experiments. To account for any asymmetry in the rocket's construction, we measured the difference between the rocket's roll with and without the battery connected (or, in the case of the statically positioned fins, by replacing the MEMS actuator with a finless one). We also measured the torsional coefficient and airflow speed for each setup.

Table 1 factors in all these measurements to calculate the output torque on the rocket body. Experimental airfoil output torque is shown to match reasonably well with the theory (Equation 2) for angles of attack under 10°, and the deviation between 10-20° angle of attack also matches the expected limit of thin airfoil theory from nonidealities. These results present a promising case for our ability to use linear control models to accurately control the rocket during flight.

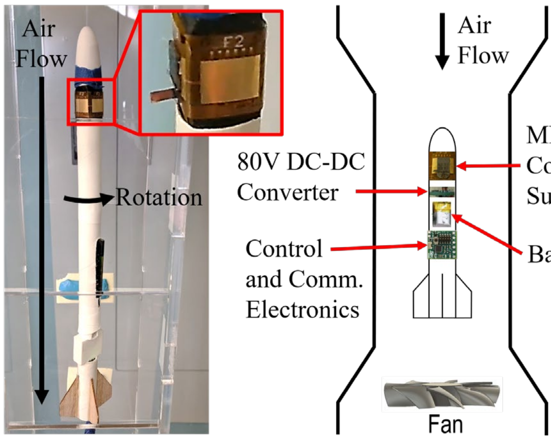

Figure 6: (Left) Lift force is generated when the fin is rotated, causing the entire rocket to roll along its axis. (Right) Schematic of the integrated rocket system inside a wind tunnel.

Angle of Attack (°)	$\tau_{roll,ideal}$ **(μNm)**	$\tau_{roll,measured}$ **(μNm)**	**σ (μNm) (N=3 trials)**
5.1[1]	4.2	3.6	0.035
10.5[2]	8.6	7.8	0.23
19.6[2]	15.8	7.8	0.13

Table 1: Output torque from the fin's lift force, measured across 3 trials for each angle of attack. All measurements were normalized to match a 2x4 mm² airfoil's area and a wind speed of 13.3 m/s. The rockets tested were either [1]electronically actuated or [2]statically positioned.

We simulated the rocket's launch performance with an Estes A3-4T engine using the software OpenRocket [13]. The rocket should have a maximum range of 360 m, a top speed of 79 m/s, and the ability to execute 10g maneuvers.

FUTURE VISION

The eventual design of a cigarette-sized rocket would comprise the Single-Chip Micro Mote (SCμM) [5] for communication and computation, an IMU for navigation, MEMS control surfaces for control, a miniaturized camera for sensing, and a rocket motor like in [4] for propulsion. The high voltage circuitry will be replaced by millimeter-scale high-voltage DC/DC converter integrated circuits [14]. Power will be supplied via two 1.5 V coin cell batteries like the SR521SW. Rocket control complexity will scale from roll stabilization using one control surface

Component	Current Dimensions (mm^3)	Current Mass (g)	Projected Dimensions (mm^3)	Projected Mass (g)
Control Surface	5 x 4 x 9	0.058	5 x 4 x 9	0.058
Battery	10 x 4 x 20	1.53	5.8 x 5.8 x 4.3	0.46
Power Circuitry	13 x 13 x 5	1.27	3 x 3 x 0.3 [14]	0.071 [14]
Control Electronics	16 x 4 x 16	1.24	2 x 3 x 0.3 [5]	0.047 [5]
Rocket Engine	13 x 13 x 45	8.5	6.4 x 6.4 x 60 [4]	1.4 [4]
Total	**15 x 15 x 201**	**19.6**	**6.4 x 6.4 x 104**	**5.7**

Table 2: Current and projected rocket volumetric dimensions and mass with future scaling of rocket components. The control surfaces presented in this paper are well suited for miniature rockets as is, and incorporating the referenced circuitry and rocket engine designs could further reduce rocket size. The total row includes the above factors plus the rocket's nose cone, electrical wiring, and fuselage.

to full roll, pitch, and yaw control using 2-4 control surfaces spaced evenly around the rocket's circumference. The rocket would be 10 cm long, 6 mm in diameter, and would have 400 m range, a top speed of 25 m/s, and the ability to execute 10g manuevers [8]. The lack of performance degradation even at lower flight speeds highlights the maneuverability improvements of rocket miniaturization. This scaling is summarized in Table 2.

CONCLUSION

We demonstrated the integration of MEMS aerodynamic control surfaces into a fully integrated miniature rocket. Improvements in assembly techniques and MEMS design substantially improved yield, helping to create MEMS aerodynamic actuators ready for use in real-world systems. These results present a promising case for the ability of MEMS aerodynamic control surfaces to sufficiently control miniature rockets during actual launches, and our higher force density actuators indicate future potential for continued size reduction.

ACKNOWLEDGMENTS

The authors would like to thank the entire Pister group and Swarm Lab. This research was financially supported by the Berkeley Sensor & Actuator Center. MEMS devices were fabricated in the Marvell Nanofabrication Laboratory at UC Berkeley.

REFERENCES

[1] D. Sathyamoorthy, "A review of security threats of unmanned aerial vehicles and mitigation steps," *Journal of Defence and Security,* October 2015, vol. 6, no. 1, pp. 81-97.

[2] D. S. Drew, B. Kilberg, and K. S. J. Pister, "Future Mesh-Networked Pico Air Vehicles," *International Conference on Unmanned Aircraft Systems (ICUAS),* June 13-16, 2017, pp. 1075–1082.

[3] D. Teasdale, "Solid Propellant Microrockets," M.S. thesis, UC Berkeley, Department of Electrical Engineering and Computer Sciences, May 2000.

[4] M. Kovač, M. Bendana, R. Krishnan, J. Burton, M. Smith, and R. J. Wood, "Multi-stage Micro Rockets for Robotic Insects," in *Robotics: Science and Systems VIII*, Sydney, Australia, 2012.

[5] F. Maksimovic et al., "A Crystal-Free Single-Chip Micro Mote with Integrated 802.15.4 Compatible Transceiver, sub-mW BLE Compatible Beacon Transmitter, and Cortex M0," *Symposium on VLSI Circuits,* June 9-14, 2019, pp. C88–C89.

[6] C. Folk and C.-M. Ho, "Micro-actuators for control of delta wing with sharp leading edge," *Aerospace Sciences Meeting and Exhibit,* January 8-11, 2001.

[7] R. J. Wood, E. Steltz, and R. S. Fearing, "Optimal energy density piezoelectric bending actuators," *Sensors and Actuators A: Physical,* April 13, 2005, vol. 119, no. 2, pp. 476-488.

[8] B. G. Kilberg, D. S. Contreras, J. Greenspun, and K. S. Pister, "MEMS aerodynamic control surfaces for millimeter-scale rockets," *International Conference on Manipulation, Automation and Robotics at Small Scales (MARSS),* August 8, 2017, pp. 1-5.

[9] B. Kilberg, D. Contreras, J. Greenspun, H. Gomez, E. Liu, and K. S. J. Pister, "MEMS Airfoil with Integrated Inchworm Motor and Force Sensor," in *Hilton Head*, Hilton Head Island, South Carolina, May 2018.

[10] C. B. Schindler, J. T. Greenspun, H. C. Gomez, and K. S. J. Pister, "A Jumping Silicon Microrobot with Electrostatic Inchworm Motors and Energy Storing Substrate Springs," *Transducers Eurosensors XXXIII*, June 23-27, 2019, pp. 88-91.

[11] S. Gutman, "Superiority of Canards in Homing Missiles," *IEEE Transactions on Aerospace and Electronic Systems*, July 2003, vol. 39, no. 3, pp. 740–746.

[12] C. B. Schindler, D. S. Drew, B. G. Kilberg, F. M. R. Campos, S. Yanase and K. S. J. Pister, "MIMSY: The Micro Inertial Measurement System for the Internet of Things," *World Forum on Internet of Things (WF-IoT),* April 15-18, 2019, pp. 329–334.

[13] Niskanen, Sampo. "Development of an Open Source model rocket simulation software," M.S. thesis, Helsinki University of Technology, Department of Engineering Physics, May 2009.

[14] J. T. Stauth, "Pathways to mm-Scale DC-DC Converters: Trends, Opportunities, and Limitations," *IEEE Custom Integrated Circuits Conference (CICC),* April 8-11, 2018, pp. 1-8.

CONTACT

A. M. Rauf, ahadrauf@berkeley.edu